Hindawi
Geofluids
Volume 2020, Article ID 9856904, 15 pages
https://doi.org/10.1155/2020/9856904

Research Article

Study on the Fractal Characteristics of Coal Body Fissure Development and the Law of Coalbed Methane Migration of around the Stope

He Yang,[1,2] Zhen Liu,[1,2] Danliang Zhu,[1,2] Wenzhi Yang,[1,2] Dawei Zhao,[1,2] and Wendi Wang[1,2]

[1]*College of Safety and Environmental Engineering, Shandong University of Science and Technology, 579 Qianwangang Rd, Huangdao District, Qingdao 266590, China*
[2]*State Key Laboratory of Mining Disaster Prevention and Control Co-founded by Shandong Province and the Ministry of Science and Technology, Shandong University of Science and Technology, Qingdao 266590, China*

Correspondence should be addressed to Zhen Liu; liuzhensdust@163.com

Received 5 February 2020; Revised 17 June 2020; Accepted 23 June 2020; Published 22 July 2020

Academic Editor: Paolo Madonia

Due to the complicated coalbed methane (CBM) occurrence conditions and the diverse geological structures in China, the promotion and application of the coal and gas simultaneous extraction technology have been seriously restricted. In view of this, this paper chooses Qingdong Coal Mine protection layer mining and CBM extraction field practice as the research background. Firstly, based on the similar material simulation experiment that simulates coal mining, the dynamic changing pattern of a mining field's overburdened strata and corresponding stress are obtained, the relationship between gas desorption and stress can then be clarified. Further, with the help of the fractal theory and box counting method, the fracture development characteristics of the overlying strata are quantitatively described on the basis of experimental images. Finally, by building a model for calculating the penetrability coefficient of coal seam based on fractal dimension of mining fissure and analyzing the relationship between fissure development and fractal dimension, the gas migration law and the fissure development areas of #7 and #8 overburden strata where CBM concentrates can be revealed and determined. According to the orientation of the area mentioned above, the location of the CBM pumping field in relation to the coal seam roof and the arrangement of CBM extraction boreholes can be optimized, which make CBM extraction efficient. Meanwhile, the risk of coal and gas outburst is significantly reduced when the CBM concentration is controlled within 0.2% to 0.6% outside the corner of the working face and 0.1% to 0.35% in return flow, which is lower than 0.8%, the threshold of CBM concentration.

1. Introduction

In recent years, with China's increasing emphasis on coal mine safety especially on the safe production of coalbed methane (CBM), for different CBM reservoir characteristics, a series of theories and techniques for mine disaster prevention and efficient green resource exploitation have been proposed [1–5]. Among all coal mine disasters, coal and gas outbursts caused by gas pressure (also known as methane pressure), ground stress, and other related factors are the biggest threat to coal mine safety [6, 7]. Therefore, effectively improving the CBM drainage rate and reducing its pressure have become the key to preventing coal and gas outburst disasters and securing the environment for coal and CBM coexploitation. China has a potential to contain significant hydrocarbon resources [8]. But due to the complicated CBM occurrence and most reservoirs are close-knit with high-gas pressure and low gas permeability, CBM exploitation is prone to trigger disasters, such as rock burst and coal and gas outbursts. Even though in soft coal seam with high ground stress, due to high gas pressure, hole collapse and plugging are also common during the construction of CBM drilling, which seriously restricts the efficiency of CBM extraction [9, 10]. It has been widely acknowledged that coal

is a porous medium with the dual fissure-pore structure like most rock masses [11, 12], the permeability of coal seam is closely related to the development of its dual fissure-pore structure [13]. Therefore, some scholars have proposed many methods to promote the porous structure development to improve CBM extraction rate, decrease the possibility of coal and gas outbursts, and achieve safe efficient simultaneous extraction of coal and gas. Under the Ostrava–Karvina Coalfield geo-mining site conditions, [14] adopted a suitable destress blasting (long-hole drilling and blasting) to prefracture the identified competent strata from both gate roads in advance. Some scholars believed that pulsating hydraulic fracturing must be carried out to improve the permeability of coal seam, and both the fissure mechanism and the gas seepage in the crack need to be studied deeply [15, 16]. [17] presented the procedures and results of numerical modelling of different stimulation methods and pointed out the hydrofracturing and jet slotting as stimulating methods can potentially enhance methane drainage from the analyzed seam. [18] combined theoretical research and field tests to exploit high-pressure air blasting for cracking and permeability enhancement. For China coal seam group mining, the protective layer mining technology is widely adopted [19, 20]. Normally, the mining of one layer contributes to the unloading of ground stress within adjacent areas and permeability increasing in nearby coal seams. Specifically speaking, this technology develops and correspondently creates fractures, thereby increasing the permeability of high-pressure and low-permeability CBM reservoirs, which ensures a better environment for CBM exploitation [21–23]. This technology relies on the find of a CBM-rich area, which is mainly based on the development of the surrounding coal and rock mass' fissures and pores, along with the CBM flow mechanism during mining processes. Some researches [24–29] show that coal, as a porous medium with a fissure-porosity dual-structure, has complex structural characteristics and obvious fractal characteristics inside of itself. Scholars use fractal dimensions to quantitatively describe the complex and disordered structure. Additionally, [30] proposed that a systematic definition of complex fractal porous media has contributed to simplifying the quantitative evaluation of multiscale structures, and the coal seam is a kind of structure with engineering properties. Meanwhile, it is believed that the distribution of the coal seam's mining-inducted fissures has strong self-similarity and fractal characteristics [31]. Therefore, it is especially simple and efficient for analyzing the fissure evolution to combine the fractal theory with the similar material simulation experiment in laboratory which can reflect the field situation well when monitoring the spatio-temporal evolution of fissures in engineering is difficult [32, 33].

According to the Qingdong Coal Mine geological prospecting report, it is found that there are 218 faults in the whole mine field. The existence of a large number of faults makes high-pressure gas gather. And the coal body in this area is soft, so the permeability of the coal seam decreases as mining depth grows. So, based on the above engineering geological conditions, an approach to achieve simultaneous coal and gas extraction through protective layer mining technology is proposed. To improve the efficiency of CBM drainage, the key of the technology is to accurately determine the CBM-rich area and rationally arrange the drainage drilling field and borehole. At present, the approximate area is generally obtained by a similar material simulation experiment combined with the gas migration theory, but the geological complexity of mining engineering tends to bring a lot of errors. Therefore, based on the similar material simulation experiment, the similar material model is corresponding to the field stratigraphic distribution, and the experimental model of similar material simulation is subdivided into 10 grids in the laboratory. And combined with the fractal box dimension method to quantitatively analyze the development degree of each grid fissure, by analyzing the relationship between fissure development, fractal dimension and gas migration law, we can accurately obtain the CBM-rich area and optimize the location of the CBM extraction field and the layout of the CBM extraction boreholes. Meanwhile, corresponding approaches can be adopted for higher CBM extraction efficiency and lower possibility of coal and gas outburst. In a nutshell, this paper attempts to put forward a new quantitative analysis method for safe coal and gas simultaneous extraction in adjacent coal seams based on similar material simulation experiment and thereby provide a new perspective for the optimization of CBM extraction and permeability enhancement in coal seams featuring high-pressure and low-permeability.

2. Brief Introduction of High Gas Pressure and Low Permeability Coal Seam Group

Qingdong Coal Mine is located in Suixi County, Huaibei City, Anhui Province, eastern China. It is dominated by coal seams No.7 and No.8 with an average total thickness of 9.23 m. The on-site measurement shows that the maximum gas pressure of coal seam No.7 is 1.8 MPa, the maximum gas content is 8.72 m^3/t•r, and its Protodyakonov's coefficient is 0.22, while the maximum gas pressure of coal seam No.8 is 1.51 MPa, the maximum gas content is 8.56 m^3/t•r, and its Protodyakonov's coefficient is 0.25. Measurements at working face 828 of working area 82 show that the permeability coefficient of the main coal seam is less than 10 mD. Therefore, coal seams No.7 and No.8 constitute a typical high-pressure and low-permeability CBM reservoir group. Taking the above geological and gas occurrence situations into consideration, this paper proposes to exploit coal seam No.7 as the upper protective layer before the exploitation of coal seam No.8, as coal seam No.7's exploitation helps fissures to develop within the coal seam and strata and forms a CBM-rich area during coal seam No.8's mining process. Then, high location drilling holes are constructed to conduct intensified CBM extraction within the CBM-rich area to reduce the gas pressure within coal seam No.8 and the risk of coal and gas outburst during mining and simultaneous coal and gas extraction. Figure 1 shows the location of the CBM reservoir group and the occurrence of coal seams and rock strata.

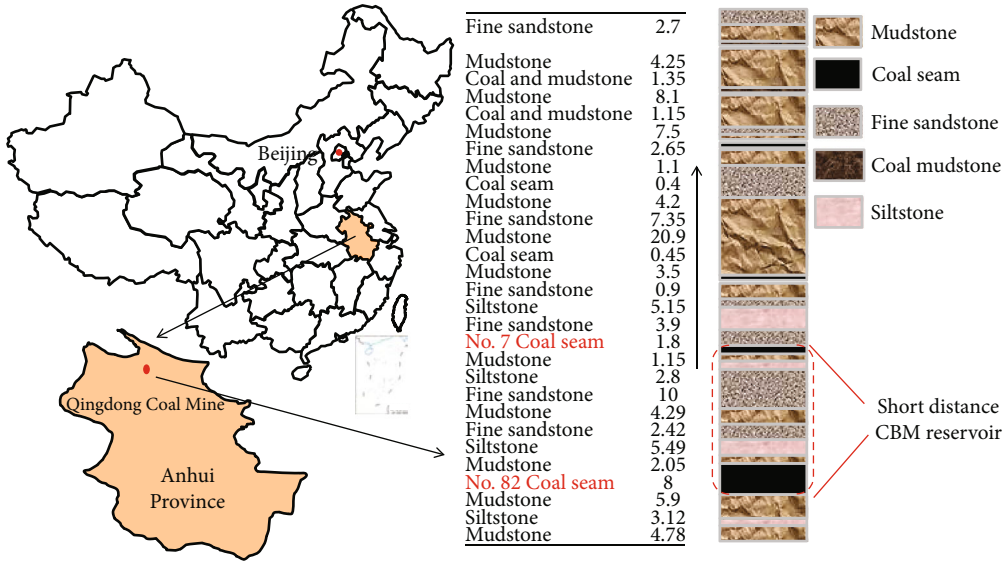

Figure 1: The CBM reservoir group and the occurrence of coal seam and rock strata.

3. Experimental Study on Spatiotemporal Evolution of Overlying Strata's Fissures

3.1. Physical Similar Material Simulation Experiment. Based on the physical similar material simulation experiment, we constructed a physical model to simulate the influence exerted by the overburden strata slumping during the mining of coal seams No.7 and No.8. The comparison between the overburden strata motion laws and fracture distribution characteristics during simultaneous mining turned out to be helpful to optimize CBM extraction in adjacent coal seams with high-pressure and low-permeability. The evolution of the key stratum plays a vital role in the process of coal-bearing strata caving because key stratum's breaking is a determining factor for rock stratum movement and mine pressure. The key stratum within the overburden strata of coal seams No.7 and No.8 can be determined with the help of a discriminant formula [34]. Then, materials such as sand, cement, gypsum, $CaCO_3$, and water are further selected as experimental aggregates. Based on the Figure 1 histogram of coal and rock, simulated rock strata are constructed according to a certain proportion of different aggregates; the specific parameters of material ratio and laying sequence are shown in Table 1.

Figure 2 demonstrates the simulation model simulating the work face during the mining process. The 2.5 m plane model frame is selected with the analogous simulation model possessing a size of $250 \times 30 \times 128$ cm (length × width × height). The similar conditions determined in our experiment are as follows:

$$\text{Geometric similarity ratio}: \alpha_l = l_p/l_m = 100 \quad (1)$$

where α_l is the geometric similarity constants; l_p stands for the prototype length; and l_m stands for the model length. Meanwhile, according to the similarity theory, the bulk density similarity constant $\alpha_\sigma = 1.6$, and the stress similarity constant $\alpha_\sigma = 160$.

3.2. Analysis of the Caving Law of Overburden Strata and Its Pressure Relief Effect during Coal Seam Mining Process

3.2.1. Overburden Movement Theory of the Goaf. The gas in the working face airflow during mining mainly comes from coal seam, goaf and adjacent coal seam; the gas emission from the goaf and adjacent coal seams mainly occurs in the coal seams mining fissures, which means a large amount of adsorbed gas is desorbed. Therefore, in order to effectively prevent coal and gas outburst disasters and improve coalbed methane drainage efficiency, it is necessary to clarify the evolution characteristics of fissures within overlying strata.

The research indicates that the damage of the overlying strata motion in the goaf of the working face is divided into bending breakage and shear failure [35]. That is, as the working face advances, the top layer of the coal seam gradually undergoes stretch bending under the stress. When the lower space permits, the bending settlement develops to the limit of the rock mass, and cracking occurs in the middle and end of the rock mass until its collapse. When the distance of the lower movement space is sufficiently large, the suspended and exposed rock formations in the middle are gradually developed from the pending settlement to fracture collapse. At the same time, the suspension beam of suspended and exposed rock formations after coal seam mining can be simplified as the embedded solid beams structure supported by the coal pillars in front of the work face, and embedded fixation is shown in Figure 3(a). The force of beam structure is provided by the upper rock layer and transmitted to the two ends of the beam, that is, the embedded part, it is judged whether the "rock beam" is cracked or broken by analyzing the stress state of the beam body.

Table 1: The specific parameters of material ratio and laying sequence.

No.	Lithology	Thickness/m	Rock total weight/kg	Sand/kg	$CaCO_3$/kg	Gypsum/kg	Water/kg	Cement/kg
1	Mudstone	4.78	38.2	30.6	5.4	2.3	4.8	
2	Siltstone	3.12	25	21.4	1.1	2.5	3.1	
3	Mudstone	5.9	47.2	37.8	6.6	2.8	5.9	
4	No. 82 coal seam	8	64	48	11.2	4.8	8	
5	Mudstone	2.05	16.4	13.1	2.3	1	2.1	
6	Siltstone	5.49	43.9	37.6	1.9	4.4	5.5	1
7	Fine sandstone	2.42	19.4	17.6		0.9	2.4	
8	Mudstone	4.29	34.3	27.5	4.8	2.1	4.3	
9	Fine sandstone	10	80	72.7		3.6	10	1
10	Siltstone	2.8	22.4	19.2	1	2.2	2.8	
11	Mudstone	1.15	9.2	7.4	1.3	0.6	1.2	
12	No. 7 coal seam	1.8	14.4	10.8	2.5	1.1	1.8	
13	Fine sandstone	3.9	31.2	28.4		1.4	3.9	
14	Siltstone	5.15	41.2	35.3	1.8	4.1	5.2	1
15	Fine sandstone	0.9	7.2	6.5		0.3	0.9	
16	Mudstone	3.5	28	22.4	3.9	1.7	3.5	
17	Coal seam	0.45	3.6	2.7	0.6	0.3	0.5	
18	Mudstone	20.9	166.8	133.4	23.4	10	20.9	
19	Fine sandstone	7.35	58.8	53.5		2.7	7.4	1
20	Mudstone	4.2	33.6	26.9	4.7	2	4.2	
21	Coal seam	0.4	3.2	2.4	0.6	0.2	0.4	
22	Mudstone	1.1	8.8	7	1.2	0.5	1.1	
23	Fine sandstone	2.65	21.2	19.3		1	2.7	
24	Mudstone	7.5	60	48	8.4	3.6	7.5	
25	Coal and mudstone	1.15	9.2	6.9	1.6	0.7	1.2	
26	Mudstone	8.1	64.8	51.8	9.1	3.9	8.1	
27	Coal and mudstone	1.35	10.8	8.1	1.9	0.8	1.4	
28	Mudstone	4.25	34	27.2	4.8	2	4.3	
29	Fine sandstone	2.7	21.6	19.6		1	2.7	

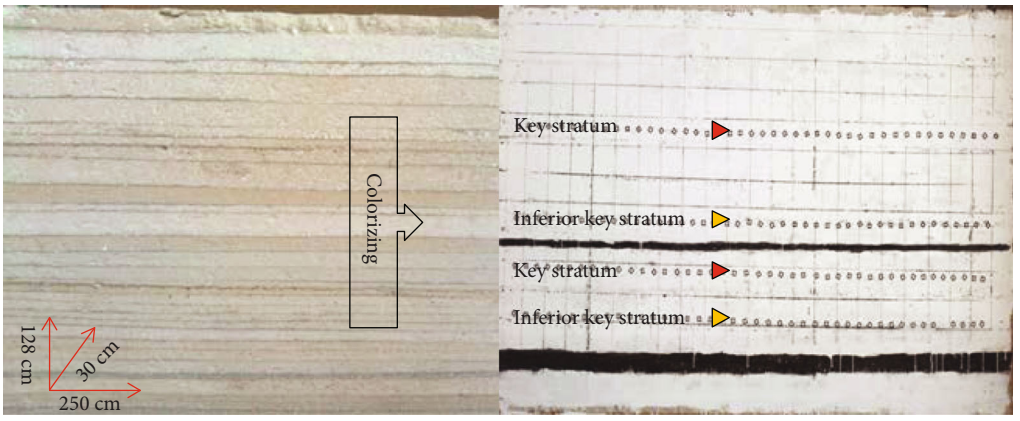

Figure 2: Model layout and key stratum location.

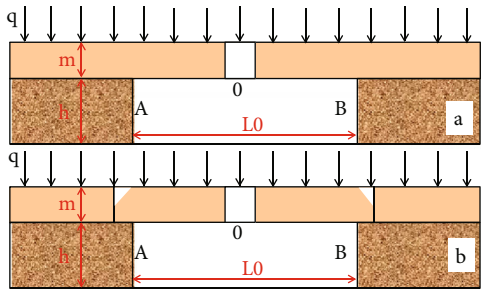

Figure 3: The model of embedded solid beams and the model of charpy force.

Taking the beam body as an example, the bending moments at the end point A and the middle point O are, respectively:

$$M_A = \frac{qL_0^2}{12} = \frac{(q_1 + q_2)L_0^2}{12}$$
$$M_0 = \frac{qL_0^2}{24} = \frac{(q_1 + q_2)L_0^2}{24} \quad (2)$$

where q_1 is the product of the bulk density of rock formation γ and the thickness m, KN/m^2; q_2 is load on the upper part of the beam $\sum_{i=1}^{n} m_i r_i$, KN/m^2; M_A, Mo is the bending moments at the end point A and the middle point O, KN·m. L_0 is the distance of suspended and exposed beam structure, m.

From the above two equations, the maximum tensile stress at the end of the beam body is:

$$\begin{cases} \sigma_A = \dfrac{M_A}{W} \geq [\sigma_t] \\ W = \dfrac{m^2}{6} \end{cases} \quad (3)$$

where W is the section modulus of the beam, m^2. σ_A is the tensile stress of point point A, Pa; m is the strata thickness, m.

Therefore, when the end of the rock mass exceeds the range of tensile force, cracking will occur, and the rock beam structure will become the model of charpy force as shown in Figure 3(b), the end bending moment will gradually decrease, and the central bending moment will start to increase. When it reaches 2 times of the initial value, the rock mass must be pulled apart, and the tensile stress value gradually develops to 3 times of the initial value until the rock mass collapses. The force analysis of this structural beam and the condition for the shear breaking of the model of charpy force is as follows.

$$\begin{cases} \tau_{\max} = [\tau] \\ \tau_{\max} = \dfrac{3Q_{\max}}{2S} \\ Q_{\max} = \dfrac{(q_1 + q_2)L_G}{2} \end{cases} \quad (4)$$

where $\tau_{\max}$ is the maximum shear stress of the beam shearing surface, Pa; $[\tau]$ is the shear strength of beam structure, Pa; $Q_{\max}$ is the maximum shear stress of beam structure, Pa; S is the shearing resisting surface of beam structure, m; L_G is the span of suspended and exposed beam structure, m.

When the tensile stress in the middle of the beam structure does not reach its limit value, the cracking surface at the end of the beam structure is insufficient due to the shear resistance, and the shear stress exceeds the limit, rock collapse occurs off. According to the breaking condition of the rock beam, it can be seen that after the formation of the goaf, due to the expansion of the caving rock and the increase of the suspension distance, the overburden layer begins to break layer by layer, which is a process that changes with space and time.

At the same time, with the mining of the working face, the overburden layer of the goaf loses its support and begins to deform, break, and collapse under the action of ground stress and self-weight, forming a region with distinct characteristics from the bottom up: caving zone, fissure zone, and bending zone, referred to as "vertical three region" [36].

Due to the different distance from the coal seam, the stress influence is also different. The rock formation near the goaf becomes a broken and discontinuous caving zone. The accumulation of fallen rock blocks in the goaf has a good supporting effect on the upper rock formation. Therefore, the rock formation in the upper part of the caving zone gradually becomes a fissure zone. As the working face advances and the goaf range gradually extends, the rock movement and the height of the fissure zone are gradually stabilized, and from the top of the fissure zone to the surface, it becomes the bending zone. Meanwhile, according to the empirical calculation method [37], the "vertical three region" distribution area of the goaf of the No.7 and No.8 coal seams in Qingdong Coal Mine can be estimated.

3.2.2. Analysis of the Caving Law of Overburden Strata and Its Fracture Development during Protected Seam Mining Process. As shown in Figure 4, coal seam No.8 was cut out 35 m from the left side of the model; excavation was carried out according to the excavation method of coal seam No.7, and then the development of fractures in its roof was observed and recorded.

As shown in Figure 4, when the working face of the model advances to 40 m, the distance of coal seam No.8's unsupported roof grows, and bed separated fissures emerge and expand due to the rock beam's large degree of settling. Once it advances to 45 m, the immediate roof begins to collapse. 50 m results in the caving of upper roof, whose breaking angle at the opening and working faces are 61° and 50°, respectively.

Some studies [35] have revealed that as the working face advances directly, the immediate roof continues to fall, and the main roof begins to experience periodic collapse. Meanwhile, fractures develop upwards due to mining, which contributes to the appearance of a large area of developed fractures above inferior key strata. When the working face advances to 55 m, the main roof begins to experience periodic collapse, and the lower part of the rock formation starts to move downward. As the working face advances to 67 m, the inferior key strata completely break, and large vertical displacement emerges. Additionally, the accumulation of the

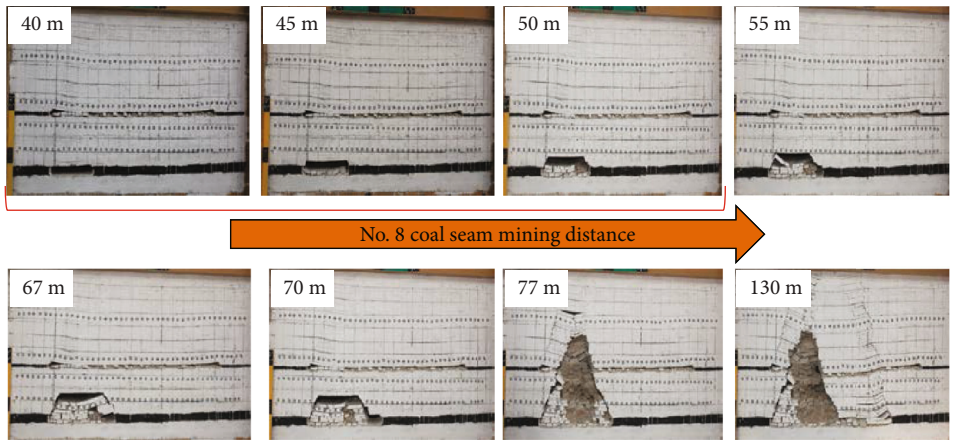

Figure 4: The law of model rock collapse during mining.

inferior key strata is more regular than that of underlying strata once it breaks. Meanwhile, the fissures develop rapidly in the soft strata above, and the breaking angle at the opening and working faces are 65° and 58°, respectively. According to the "vertical three region" theory [36], the height of the caving is 15 m, and the fissure zone is up to 23 m high. When the working surface advances to approximately 75 m, the main key stratum helps to support the caving strata from the goaf of coal seam No.7 above due to its higher strength. Therefore, the inferior key strata act as a cantilever beam structure at the working surface after breaking, which is attributed to the increase of the caving span of the goaf's overlying strata. Afterwards, at 77 m, the length growth of the overhanging strata in the goaf, the collapses periodically of inferior key strata as the working face advances increases the risk of caving that leads to the breaking of the coal seam No.8's key-stratum and subsequent movement of a large number of broken strata in the overlying strata. Under the circumstance, the originally compacted and closed fissures are reopened due to the mining process. At this spot, the breaking angle at the open-off cut and the working surface are 65° and 58°, respectively. The height of the caving zone is 27 m, while the height of the fissure zone is 79 m. When the excavation of model proceeds to 130 m, it can be clearly observed that the rock beams at the open-off cut and the working face have broken into trapezoidal structure, and fissures are fully developed in the waistline region of the trapezoidal structure. Meanwhile, the main key stratum of coal seam No.8 demonstrates obvious bending and sinking, similar to that of a masonry beam, the arrangement of broken fissures is relatively even, and the breaking angle at the open-off cut and the working surface are 67° and 65° at 130 m, respectively. Caving zone's height ranges between 25 m and 27 m, and the fissure zone is approximately 79 m high, which is mainly distributed in the upper layer of coal seam No.7's goaf. Therefore, we believe that during the mining process of coal seam No.8, the breaking of the key strata can easily affect the caving zone of coal seam No.7's goaf, that is, it helps form a secondary mining-affected area with a wide range of influence and a large free space in a very short time and create conditions for the formation of CBM-rich area.

3.2.3. Analysis of Pressure Relief Effect after Adopting Protective Layer Mining. To monitor the change under stress in coal seam No. 8 during the mining of coal seam No.7, 4 stress sensors were laid in the roof of the simulated coal seam No. 8 in our simulation experiment. Initially, the sensor value was set to zero, and Figure 5 demonstrates the change in coal seam No. 8 as coal seam No.7's working face proceeds.

As shown in Figure 5, the stress begins to gradually increase as coal seam No.7's working face advances closer to the measurement point, indicating that coal seam No.8 is affected by the mining of coal seam No.7. To be more specific, the strata above coal seam No.8 begin to expand and the pressure gradually reduces. As coal seam No.7's working face advances, the stress grows and reaches its climax, and coal seam No.8's pressure relief effect would demonstrate its full strength. Further, due to the caving and compaction of coal seam No.7's overlying strata, the stress value gradually decreases after reaching the maximum. It was noticed during our experiment that sensor 1, 2, 3, and 4 began to demonstrate depressurization when they were 23.5 m, 19.5 m, 25 m, and 25 m ahead of coal seam No.7's working face, respectively. Additionally, sensor 1, 2, 3, and 4 records its climax stress value at 25.5 m, 23.5 m, 26.5 m, and 26 m, respectively, indicating that when the working face of coal seam No.7 (protective layer) is pushed to this distance, the pressure of coal seam No.8 is sufficiently relieved. Therefore, we conclude that the depressurization of coal seam No.8 caused by the mining of coal seam No.7 will be beneficial to the desorption of a large amount of adsorbed gas, ensuring the safety growth of the CBM extraction volume and the effective reduction of the gas pressure.

4. Analysis of Evolution Law of Mining Fissures Based on Fractal Theory

4.1. Quantitative Characterization Method of Fissure Development Based on Fractal Geometry Theory. As shown in Figure 6, coal seam No.8 has been mined for 130 m. According to above conclusions, the overlying migration strata are divided into two 24 m long slanted strips that are parallel to the breaking line [38], and then the inclined strips

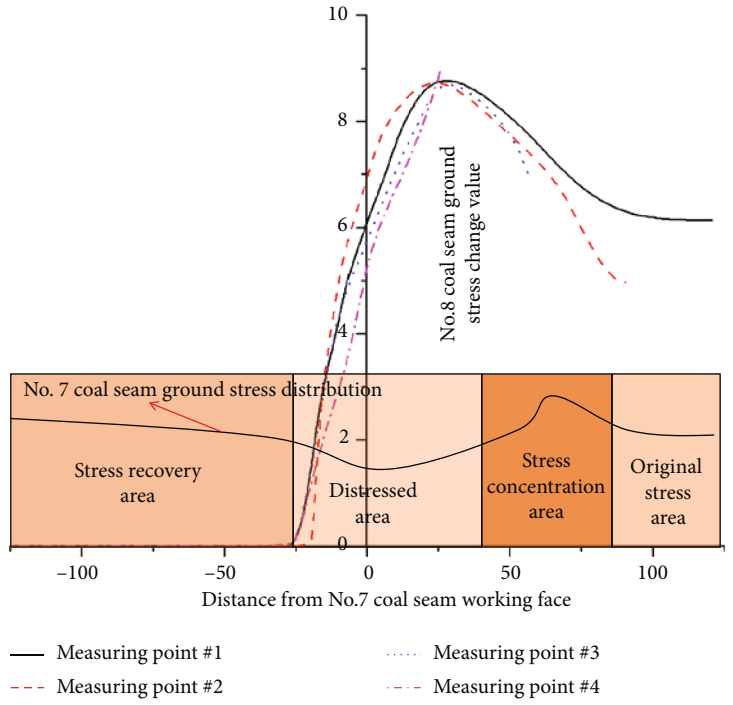

Figure 5: The figure of stress measuring points.

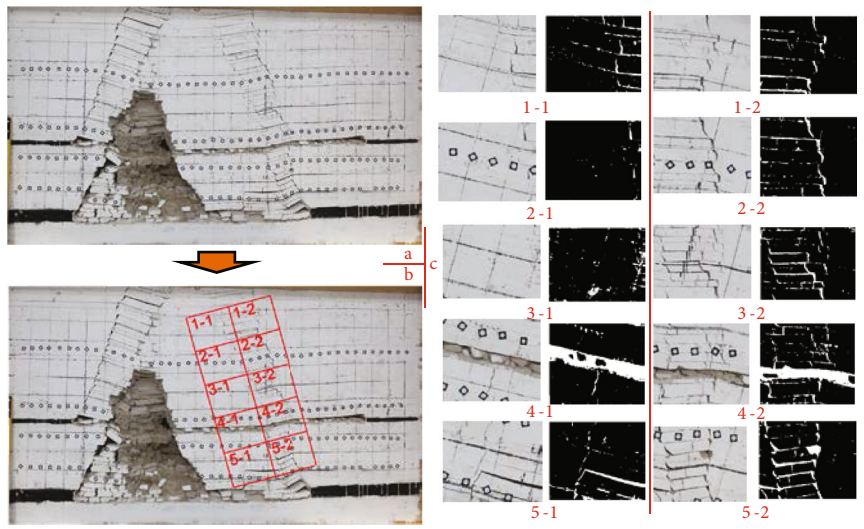

Figure 6: Meshing image of overlying strata. (a) Original picture. (b) Mesh distribution. (c) Mesh after binarization.

are further divided into 10 grids with a height of 20 m in the direction perpendicular to the breaking line before they are numbered; the center orientation of each grid is as shown in Table 2. Then, the values are introduced into MATLAB software in turn and preprocessed into grayscale images according to the image features, and a fast Fourier forward/inverse transform and ideal low-pass filter are used to adjust different cutoff frequencies, D_0, to filter the high-frequency portion and obtain multiple filtering enhanced images. The optimal cutoff frequency D_0 is 250. Then, the thresholds are determined by an iterative method to obtain a binarized image. Finally, the definition of the observation scale (with a square side length of 2 to 110 pixels) based on the box counting method is determined to find the fractal model of the fissure structure [39]. Therefore, we can obtain the macro-meso structure's surface area fractal dimensions for the coal and rock mass during the mining process, thereby analyzing the relationship between the development degree of mining fissures and the fractal dimension.

4.2. Fractal Dimension Measurement Results and Analysis. The calculation results of porosity and fractal dimension of each grid are shown in Figure 7.

It can be seen from Figure 7 that the fractal dimension has a positive correlation trend with the increase of porosity, that is, the fractal dimension becomes larger as the degree of

Table 2: Grid distances.

Grids	Vertical distance from coal seam No.8's floor (m)	The distance from foot of perpendicular to coal seam No.8's opening (m)	Grids	Vertical distance from coal seam No.8's floor (m)	The distance from foot of perpendicular to coal seam No.8's opening (m)
1-1	93.73	71.03	1-2	99.52	94.96
2-1	74.87	76.53	2-2	80.66	100.46
3-1	56.01	82.03	3-2	61.80	105.96
4-1	37.15	87.53	4-2	42.94	111.46
5-1	18.29	93.03	5-2	24.08	116.96

development of mining fissures increases. Therefore, the fractal dimension obtained from the similar material simulation experiment image can quantitatively describe the development of the overlying strata's mining-inducted fissures. According to the curves in the figure, it is considered that mining-inducted fissures develop better in the region where grids 3-2, 4-1, 4-2, and 5-2 are located than in other regions. Theoretically [40, 41], the abovementioned fissure development regions can provide sufficient space for the desorption of adsorbed gas and the flow of free gas within the coal seam, and the similar material simulation experiment model shows that the area where grid 4-1 and 4-2 are located in coal seam No.7's mining area. At the same time, the goaf area may be mistakenly identified as a fissure area during measurement, and the calculation results also show that the fractal dimension is greater than 1.9 and close to 2. Therefore, according to the actual situation, the area where the two grids are located cannot be defined as the CBM enrichment area.

4.3. Relationship between the Penetrability Coefficient and the Fractal Dimension. [42] made an analogy between coarse spots or bulges on the surfaces of islands or buildings on earth and pores in a porous medium and obtained the fractal scaling law for fissure size distribution in a porous medium:

$$-dN = D\lambda_{\max}^{D}\lambda^{-(D+1)}d\lambda \tag{5}$$

where N is the number of fissures with a diameter exceeding λ; D is the fractal dimension of the fissure area, which is represented as a function of the porous medium porosity n, maximum fissure diameter $\lambda_{\max}$ and minimum fissure diameter $\lambda_{\min}$.

Therefore, the porous medium porosity can be calculated by the theoretical fissure area fractal dimension:

$$\mathrm{n} = (\lambda_{\min}/\lambda_{\max})^{2-D} \tag{6}$$

Due to the influence of mining, the porosity of each region is different, the influence factors of the porosity are expressed in Equation (6), the microcells inside the goaf are defined as isotropic medium, and the penetrability coefficient can be calculated by Kozeny-Carman [3]:

$$e = a\frac{n^3}{(1-n)^2 M_s^2} \tag{7}$$

where e is the penetrability coefficient; a is the empirical coefficient, value is 0.2; n is the porosity; M_S is the specific surface area of pore skeleton in porous media, m.

Bringing Equation (6) to Equation (7), the relationship between fractal dimension and penetrability coefficient can be given:

$$e = a\frac{(\lambda_{\min}/\lambda_{\max})^{3(2-D)}}{\left[1-(\lambda_{\min}/\lambda_{\max})^{2-D}\right]^2 M_s^2} \tag{8}$$

According to the above law of development of mining fissures, when the minimum fissure diameter is fixed, the maximum fissure diameter and fractal dimension become larger as the degree of development of mining fissures increases. At the same time, it can be seen from Equation (8) that the penetrability coefficient of the coal seam also increases with the increase of the fractal dimension and the maximum diameter of the fissure, that is, the region with larger fractal dimension is more favorable for the desorption and migration of gas, thereby forming the CBM-rich area.

4.4. CBM-Rich Area Determination. Based on above analysis, after the mining of coal seam No.7, a CBM accumulation area emerges at the area where grid 3-2 is located. The main reason for this is that with the continuous advancement of coal seam No.7's working face, the inferior key stratum bends gradually, and the soft rock stratum loses its support, resulting in a large number of separation cracks in the soft rock between the inferior key stratum and the main key stratum in the upper part of coal seam No.7. Afterwards, when the main key stratum gradually begins to bend and break, a large number of lateral and vertical fissures appear in the lower strata of the main key stratum of coal seam No.7. Further, the CBM accumulation area is gradually formed in the area where the 3-2 grid is located under the stratum stress provided by the periodic break of the upper roof. The formation of the CBM-rich area will facilitate the migration and diffusion of high-pressure gas within coal seam No.8, providing a prerequisite for the safer mining of coal seam No.8. The area where grid 5-2 is located is in the CBM accumulation area of coal seam No.8. The formation of this area is mainly due to the breaking of the main key stratum of coal seam No.8 and its large-scale impact out from suddenly sinking onto the overburden strata that have been broken or are going to be broken. Meanwhile, the sinking of the key stratum of coal seam No.7 is a continuous process, and the strata

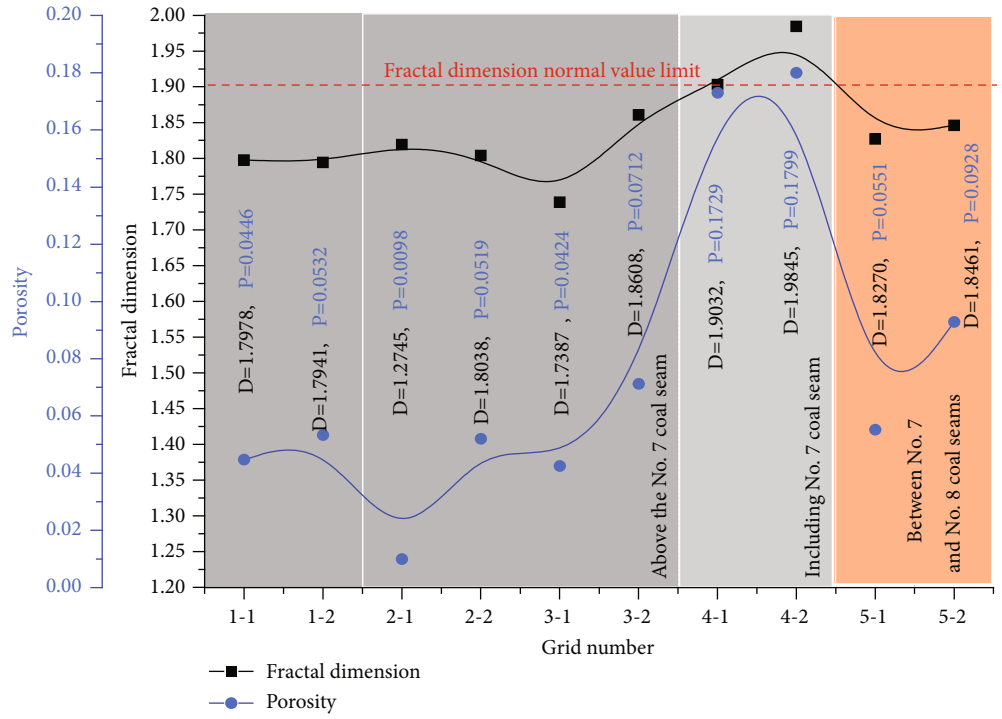

(a)

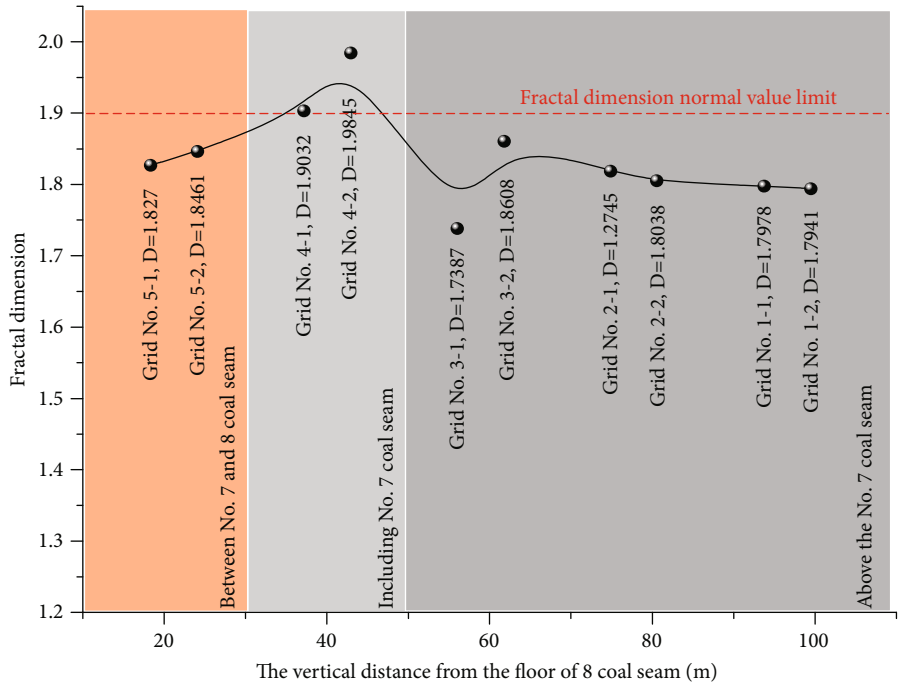

(b)

Figure 7: Continued.

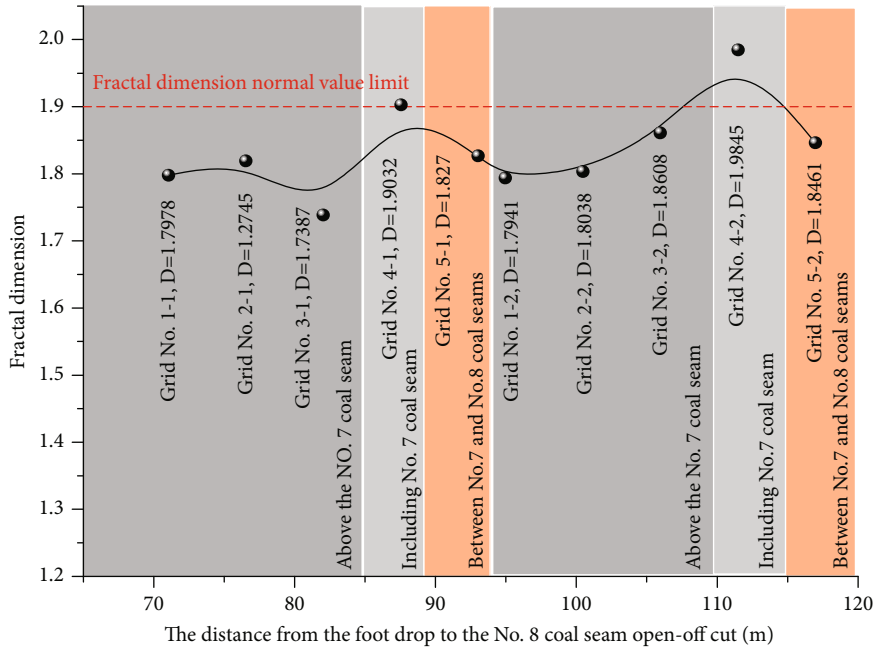

(c)

Figure 7: The calculation results of porosity and fractal dimension of each grid. (a) The relationship between fractal dimension and porosity. (b) The relationship between fractal dimension and vertical distance from coal seam No.8's floor. (c) The relationship between the fractal dimension and the distance from foot of perpendicular to coal seam No.8's.

underneath will experience a large-scale sinking movement as the key stratum of coal seam No.8 sinks. It is obvious that the movement of a large number of strata underneath is attributed to the formation of a large number of fissures, which also helps the formation of the CBM accumulation area.

The movement of the abovementioned overburden strata and the formation of the fissure zone will further connect the primary and secondary fissures, providing channels for gas circulation, causing a sudden decrease of the gas pressure within the region, and forming a pressure difference between the upper and lower portions, which enables CBM to flow into the region. Meanwhile, the CBM in the upper portion of the coal seam No.7's fissure zone and the goaf of coal seam No.8 simultaneously flow into the region and form a CBM accumulation area. Additionally, the periodic breaking of the coal seam No.8's key stratum forms a respiration zone between the strata, so that the CBM continuously accumulates. Therefore, the CBM extraction in the area can reduce the CBM content on the one hand and form the negative pressure on the other hand to maintain the CBM pressure and flow within the region. Overall, it helps the CBM to migrate along the fissure zone into free space, thereby reducing the CBM emission at the working face.

5. Engineering Application

5.1. Practice at CBM Extraction Field. According to the experimental results which are the quantitative analysis of the fissure development in the subregion and the actual situation on the site, in order to further improve the CBM extraction rate and solve gas pressure overrun at coal seam No.8's working face after depressurization, it is necessary to construct an upper drilling field between coal seams No.7 and No.8 to perform lower interception and extract the CBM concentrated at the low, thereby fulfilling safe coal and gas mining. The final boreholes shown in Figure 8 lie in deep area where grid 5-2 is located.

When designing the drilling field, the height of the high-level borehole should be determined according to the formation characteristics of the secondary mining-affected area and the distance from coal seam No.7's goaf to coal seam No.8's roof. Therefore, taking the distribution of mining-inducted fissures within coal seam No.8's roof into consideration, we intend to control the hole bottom position within the range of grid 5-2. According to the analysis, the high-level boreholes are staggered in parallel, that is, the front and the latter row of boreholes share the same normal length while having different horizontal distances, and the front row is 40 m ahead, relatively. The actual construction parameters of the upper drilling field are shown in Table 3.

5.2. Analysis of Intensified CBM Extraction. To fully demonstrate the relationship between the location of the borehole and the average extraction concentration within the borehole, as shown in Figure 9(a), the average concentration within each borehole in the stope during the CBM extraction period is recorded during the field test. For the purpose of further analyzing the influence of mining on CBM extraction, the variation of the mixed gas concentration in the drilling field No.1 and No.2 during the extraction is as shown in Figure 9(b). Furthermore, Figure 9(c) illustrates the gas

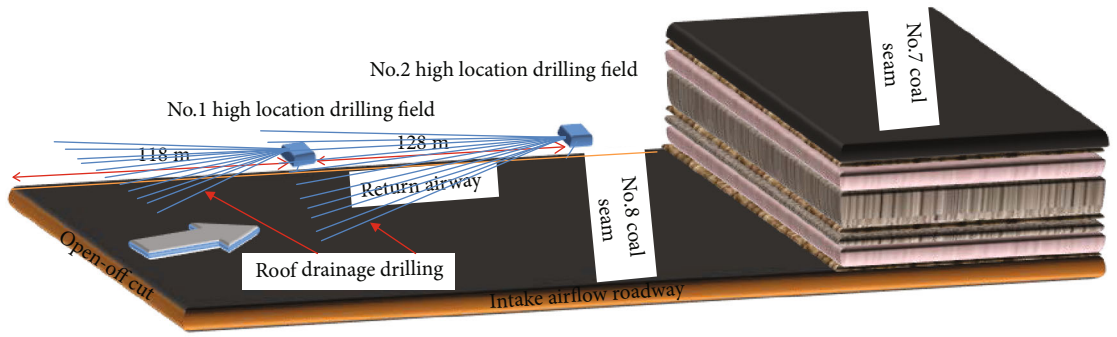

Figure 8: Layout of upper drilling fields.

Table 3: Actual construction parameters of upper drilling field.

No.1 high location drilling field						No.2 high location drilling field					
No.	ND	HD	D	A	DA	No.	ND	HD	D	A	DA
1	22.61	5	100.5	275.7	13	1	20	5.5	143	269	3.5
2	20.90	13	100.5	278	12	2	19.5	10.9	143.5	271	3
3	21.64	21	100	283	12.5	3	20.5	18.7	141	274	3
4	18.31	29	100.5	289	10.5	4	20.4	26.6	142.5	277	2.5
5	20.80	35	126	273	9.5	5	17.6	26.4	96	278	2
6	22.57	9	130	276	10	6	23.5	32.9	106.5	281	4.5
7	21.46	17	130	280	9.5	7	16.6	3.7	100.5	266	5.5
8	20.34	25	130	284	9	8	17.8	11.9	90	270	5
9	13.12	31	100.5	274	7.5	9	19.5	18.5	98.5	274	4.5
10	15.17	40	124.5	280	7	10	16.4	27.8	92	279	4
11	10.71	41	101.9	286	6	11	15.5	33.2	93.5	282	3

ND: normal distance is the vertical distance between the axial end position of the high-level borehole and the top boundary of coal seam No.8, *m*; HD: the horizontal distance is the vertical distance between the projection point of the high-level borehole in the horizontal plane and the lane of the return air passage of the working face, *m*; D: depth, *m*; A: azimuth, °; DA: dip angle, °.

concentration at the working face's upper corner and return air way when drilling field No.2 is operational.

It can be seen from Figure 9(a) that the 2 lowest average concentrations of gas extraction are recorded from drilling hole No.1 and No.7, whose vertical distances are 3.7 m and 5.5 m and normal distances are 20 m and 16.7 m, respectively. According to the analysis of the position where these two drilling holes end, we found that they are both located outside the area where CBM accumulates. Additionally, fissures are under development in the specific outer areas, which is attributed to the lower gas concentration over an extended period. At the same time, during the coal and gas coextraction, as the working face advances, the position where the end of drilling holes will gradually decrease as the overlying strata caves, while the gas concentration increases during the extraction.

As shown in Figure 9(b), at the beginning of mining, the CBM concentration in drilling field No.1 is low, with the maximum mixing concentration registering of 9.2%, and the minimum of 2.4%. As the drilling field No.1 begins operation, the CBM concentration gradually decreases. As the working face approaches the compression area, drilling field No.2 starts to work. At the beginning, the CBM concentration is lower than that of drilling field No.1. As the working face continues to advance, it gradually exceeds that of drilling field No.1, with the maximum CBM concentration registering of 15.6% and the minimum concentration of 2.3%. The explanation is that the height of coal seam No.8's caved roof is low, the caving zone possesses a low stacking height, and fissures are under development at the start of the mining process. At this stage, vertical fissures have not yet connected with the coal seam No.7's goaf, and the gas has not yet accumulated in this area. Therefore, in the initial stage of mining, only the CBM reserved in coal seam No.7's goaf has been extracted by drilling field No.1, and the overall extraction efficiency is low. With the strata's total collapse at the working face, the normal distance of the drilling holes gradually decreases into the air leakage area, and this action is responsible for the gradual decline in gas concentration during extraction.

As shown in Figure 9(c), the gas concentration in the working face's upper corner during the extraction of the drilling field No.2 is between 0.2% and 0.6%, with an average of 0.34%. Meanwhile, the return air flow concentration is within 0.1% to 0.35%, with an average of 0.16%. Both the values are lower than the gas alarm value, 0.8%. Therefore, the

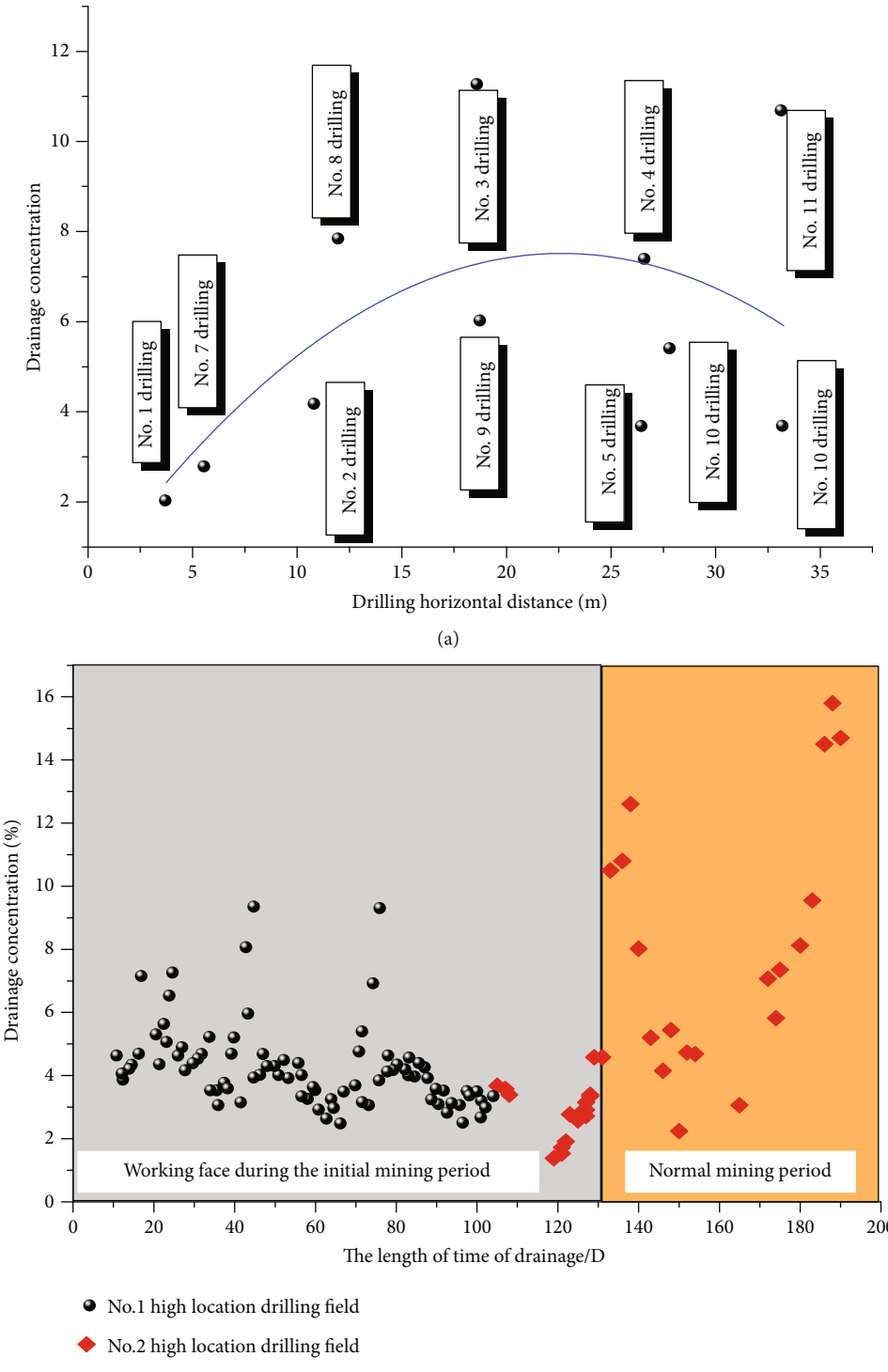

(a)

(b)

Figure 9: Continued.

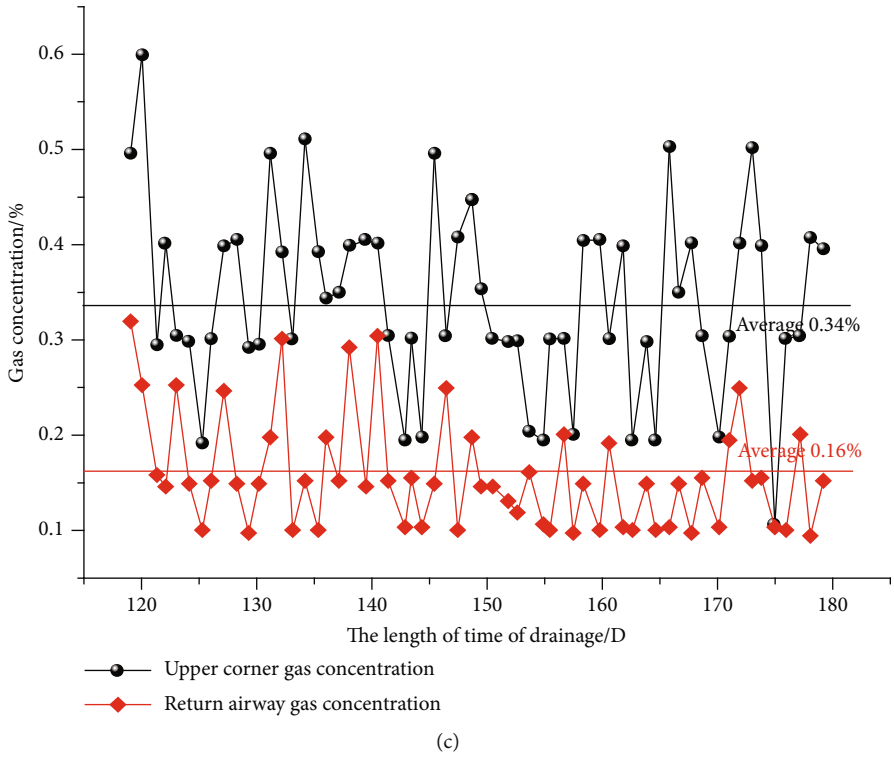

Figure 9: Drilling and drainage concentration level from the diagram.

extraction of high-level boreholes significantly inhibits the accumulation of gas at the upper corner of the working face and reduces the concentration of gas leaking out from goafs. This approach guarantees a safe and efficient implementation of coal and gas co-extraction in Qingdong Coal Mine.

6. Conclusions

(1) Based on the experimental images calculated and processed by the fractal theory and box counting method, the calculation results show that there is a positive correlation between the porosity and fractal dimension of each grid in the area affected by mining. Meanwhile, the penetrability coefficient of the coal seam increases with the increase of the fractal dimension and the maximum diameter of the fissure, so the region with the larger fractal dimension is more favorable for the desorption and migration of CBM

(2) Industrial gas extraction experiments show that the average concentration of gas at the upper corner and the return airway register of 0.34% and 0.16%, respectively, which are both lower than the alarm threshold of 0.8%. Thus, the CBM extraction efficiency can be significantly improved, the risk of coal and gas outburst can be reduced and the safe and efficient coal and gas coextraction can be ensured by pinpointing the location of the construct upper drilling fields and the drilling holes end

Data Availability

The research data used to support the findings of this study may be released upon application to the corresponding author Dr. Zhen Liu, who can be contacted at liuzhensdust@163.com. Some or all data, models, or code generated or used during the study are available from the corresponding author by request. (Experimental equipment parameters, laboratory experimental results data, field experimental results, etc.).

Conflicts of Interest

The authors declare that there is no conflict of interest regarding the publication of this paper.

Acknowledgments

The authors would like to acknowledge the support of the National Natural Science Foundation of China (No.51604168, 51934004, 51904171), Major Program of Shandong Province Natural Science Foundation (NO. ZR2018ZA0602), the Key Research and Development Plan of Shandong Province, China (No.2019GSF111033), Taishan Scholars Project Special Funding (TS20190935), Innovation Fund-funded Projects of Postgraduate of Shandong University of Science and Technology (No. SDKDYC190117).

References

[1] Y. Li, C. Zhang, D. Tang et al., "Coal pore size distributions controlled by the coalification process: an experimental study

of coals from the Junggar, Ordos and Qinshui basins in China," *Fuel*, vol. 206, pp. 352–363, 2017.

[2] K. Noack, "Control of gas emissions in underground coal mines," *International Journal of Coal Geology*, vol. 35, no. 1-4, pp. 57–82, 1998.

[3] B. A. Poulsen, D. Adhikary, and H. Guo, "Simulating mining-induced strata permeability changes," *Engineering Geology*, vol. 237, pp. 208–216, 2018.

[4] J. Stopa and S. Nawrat, "Computer modeling of coal bed methane recovery in coal mines," *Journal of Energy Resources Technology*, vol. 134, no. 3, 2012.

[5] G. Zhou, Y. Ma, T. Fan, and G. Wang, "Preparation and characteristics of a multifunctional dust suppressant with agglomeration and wettability performance used in coal mine," *Chemical Engineering Research and Design*, vol. 132, pp. 729–742, 2018.

[6] B. B. Huoduote, *Coal and Gas Outburst, Translated by Song SZ and Wang YA*, China Industry Press, Beijing, 1966.

[7] N. Kursunoglu and M. Onder, "Application of structural equation modeling to evaluate coal and gas outbursts," *Tunnelling and Underground Space Technology*, vol. 88, pp. 63–72, 2019.

[8] Y. Li, J. H. Yang, Z. J. Pan, S. Z. Meng, K. Wang, and X. L. Niu, "Unconventional natural gas accumulations in stacked deposits: a discussion of Upper Paleozoic coal-bearing strata in the east margin of the Ordos Basin, China," *Acta Geologica Sinica-english Edition*, vol. 93, no. 1, pp. 111–129, 2019.

[9] C. J. Fan, S. Li, M. K. Luo, Z. H. Yang, H. H. Zhang, and S. Wang, "Deep CBM extraction numerical simulation based on hydraulic-mechanical-thermal coupled model," *Journal of China Coal Society*, vol. 12, pp. 3076–3085, 2016.

[10] H. Li and G. S. Hao, "Deep hole drilling technology tailored for gas drainage in soft seams in high outburst mines," *Journal of Heilongjiang University of Science & Technology*, vol. 29, no. 6, pp. 642–647, 2019.

[11] Z. Liu, H. Yang, W. Wang, W. Cheng, and L. Xin, "Experimental study on the pore structure fractals and seepage characteristics of a coal sample around a borehole in coal seam water infusion," *Transport in Porous Media*, vol. 125, no. 2, pp. 289–309, 2018.

[12] Z. Liu, W. Wang, W. Cheng, H. Yang, and D. Zhao, "Study on the seepage characteristics of coal based on the Kozeny-Carman equation and nuclear magnetic resonance experiment," *Fuel*, vol. 266, 117088 pages, 2020.

[13] T. Kubo, N. Matsuda, K. Kashiwaya et al., "Characterizing the permeability of drillhole core samples of Toki granite, Central Japan to identify factors influencing rock-matrix permeability," *Engineering Geology*, vol. 259, p. 105163, 2019.

[14] P. Konicek, K. Soucek, L. Stas, and R. Singh, "Long-hole destress blasting for rockburst control during deep underground coal mining," *International Journal of Rock Mechanics & Mining Sciences*, vol. 61, pp. 141–153, 2013.

[15] M. A. A. Ahamed, M. S. A. Perera, L. Dong-yin, P. G. Ranjith, and S. K. Matthai, "Proppant damage mechanisms in coal seam reservoirs during the hydraulic fracturing process: a review," *Fuel*, vol. 253, pp. 615–629, 2019.

[16] N. Guanhua, D. Kai, L. Shang, and S. Qian, "Gas desorption characteristics effected by the pulsating hydraulic fracturing in coal," *Fuel*, vol. 236, pp. 190–200, 2019.

[17] W. Szott, M. Słota-Valim, A. Gołąbek, K. Sowiżdżał, and P. Łętkowski, "Numerical studies of improved methane drainage technologies by stimulating coal seams in multi-seam mining layouts," *International Journal of Rock Mechanics and Mining Sciences*, vol. 108, pp. 157–168, 2018.

[18] K. W. Wang, "Study on technology of fracturing and permeability improved of coal seam with high pressure air blasting," *Coal Science and Technology*, vol. 46, no. 2, pp. 193–197, 2018.

[19] J. Brandt and R. Sdunowski, "Gas drainage in high efficiency workings in German Coal mines," in *Proceeding of 2007' China (Huainan) international symposium on coal gas control technology*, pp. 22–29, China University of Mining and Technology Press, Xuzhou, 2007.

[20] Z. Liu, H. Yang, W. Cheng, L. Xin, and G. Ni, "Stress distribution characteristic analysis and control of coal and gas outburst disaster in a pressure-relief boundary area in protective layer mining," *Arabian Journal of Geosciences*, vol. 10, no. 16, p. 358, 2017.

[21] B. B. Beamish and P. J. Crosdale, "Instantaneous outbursts in underground coal mines: an overview and association with coal type," *International Journal of Coal Geology*, vol. 35, no. 1-4, pp. 27–55, 1998.

[22] A. M. S. Iwanec, J. P. Carter, and J. P. Hambleton, "Geomechanics of subsidence above single and multi-seam coal mining," *Journal of Rock Mechanics and Geotechnical Engineering*, vol. 8, no. 3, pp. 304–313, 2016.

[23] B. Q. Lin and H. X. Cui, *Mine Gas Prevention and Control Theory and Technology*, China University of Mining and Technology Press, Xuzhou, 1998.

[24] Z. Liu, W. Wang, H. Yang, D. Zhao, and W. Wang, "Experimental study on spontaneous imbibition characteristics of coal based on fractal theory," *Advanced Powder Technology*, vol. 31, no. 5, pp. 1994–2004, 2020.

[25] A. D. Alekseev, T. A. Vasilenko, and A. K. Kirillov, "Fractal analysis of the hierarchic structure of fossil coal surface," *Journal of Mining Science*, vol. 44, no. 3, pp. 235–244, 2008.

[26] S. Chen, Z. Du, Z. Zhang, H. Zhang, Z. Xia, and F. Feng, "Effects of chloride on the early mechanical properties and microstructure of gangue-cemented paste backfill," *Construction and Building Materials*, vol. 235, 2020.

[27] Y. Li, J. Yang, Z. Pan, and W. Tong, "Nanoscale pore structure and mechanical property analysis of coal: an insight combining AFM and SEM images," *Fuel*, vol. 260, 2020.

[28] M. M. Mahamud and M. F. Novo, "The use of fractal analysis in the textural characterization of coals," *Fuel*, vol. 87, no. 2, pp. 222–231, 2008.

[29] H. Yang, W. Cheng, Z. Liu, W. Wang, D. Zhao, and W. Yang, "Study on the dynamic evolution law of the effective stress in the coal seam water infusion process based on fractal theory," *Fractals*, 2020.

[30] Y. Jin, C. Wang, S. Liu, W. Quan, and X. Liu, "Systematic definition of complexity assembly in fractal porous media," *Fractals*, 2020.

[31] K. N. Trubetskoy, A. D. Ruban, S. D. Viktorov et al., "Fractal structure of deformed coal beds and their susceptibility to gas-dynamic failure," *Doklady Earth Sciences*, vol. 431, no. 2, pp. 538–540, 2010.

[32] H. Y. Li, W. H. Wang, Q. X. Qi, and L. Zhang, "Study on fissure development rule of overlying strata influenced by mining based on fractal theory," *Journal of China Coal Society*, vol. 39, no. 6, pp. 1023–1030, 2014.

[33] D. Mondal and P. N. S. Roy, "Fractal and seismic b-value study during dynamic roof displacements (roof fall and surface

blasting) for enhancing safety in the longwall coal mines," *Engineering Geology*, vol. 253, pp. 184–204, 2019.

[34] M. G. Qian, X. X. Liao, and J. L. Xu, "Theoretical study of key stratum in ground control," *Journal of China Coal Society*, vol. 21, no. 3, pp. 225–230, 1996.

[35] Y. L. Tan, *Mine pressure and strata control*, China Coal Industry Publishing House, Beijing, 2010.

[36] M. G. Qian, P. W. Shi, and J. L. Xu, *Mine Pressure and Rock Formation Control*, China University of Mining and Technology Press, Xuzhou, 2010.

[37] G. H. Shen, B. Y. Li, and G. Wu, *Theory and Practice of Special Mining in Mines*, China Industrial Press, Beijing, 1992.

[38] G. Wang, M. Wu, R. Wang, H. Xu, and X. Song, "Height of the mining-induced fractured zone above a coal face," *Engineering Geology*, vol. 216, pp. 140–152, 2017.

[39] C. Panigrahy, A. Seal, N. K. Mahato, and D. Bhattacharjee, "Differential box counting methods for estimating fractal dimension of gray-scale images: a survey," *Chaos, Solitons & Fractals*, vol. 126, pp. 178–202, 2019.

[40] A. Burra, J. S. Esterle, and S. D. Golding, "Use of temperature logs in coal seam gas reservoirs: application to the Sydney Basin, Australia," *International Journal of Coal Geology*, vol. 143, pp. 68–77, 2015.

[41] S. S. Raza, L. Ge, T. E. Rufford, Z. Chen, and V. Rudolph, "Anisotropic coal permeability estimation by determining cleat compressibility using mercury intrusion porosimetry and stress-strain measurements," *International Journal of Coal Geology*, vol. 205, pp. 75–86, 2019.

[42] B. M. Yu, P. Xu, M. Q. Zou, J. C. Cai, and Q. Zheng, *Fractal Porous Media Transport Physics*, Science Press, Beijing, 2014.